Earth and Planetary Science Letters 459 (2017) 279–290

Contents lists available at ScienceDirect

Earth and Planetary Science Letters

www.elsevier.com/locate/epsl

Resolving depth-dependent subduction zone viscosity and afterslip from postseismic displacements following the 2011 Tohoku-oki, Japan earthquake

Andrew M. Freed[a,*], Akinori Hashima[b], Thorsten W. Becker[c,d], David A. Okaya[c], Hiroshi Sato[b], Yuki Hatanaka[e,d]

[a] Department of Earth, Atmospheric, and Planetary Sciences, Purdue University, West Lafayette, IN, USA
[b] Earthquake Research Institute, The University of Tokyo, Yayoi, Bunkyo-ku, Tokyo 1130032, Japan
[c] Department of Earth Sciences, University of Southern California, Los Angeles, CA, USA
[d] Jackson School of Geosciences, The University of Texas, Austin, TX, USA[1]
[e] Geospatial Information Authority of Japan, 1 Kitazono, Tsukuba, Ibaraki, 305-0811, Japan

A R T I C L E I N F O

Article history:
Received 2 April 2016
Received in revised form 30 August 2016
Accepted 21 November 2016
Available online 7 December 2016
Editor: B. Buffett

Keywords:
postseismic
Tohoku-oki
viscoelastic relaxation
afterslip
finite element modeling

A B S T R A C T

We developed a 3-D, viscoelastic finite element model of the M9 2011 Tohoku-oki, Japan earthquake capable of predicting postseismic displacements due to viscoelastic relaxation and afterslip. We consider seismically inferred slab geometries associated with the Pacific and Philippine Sea Plate and a wide range of candidate viscoelastic rheologies. For each case, we invert for afterslip based on residual surface displacements (observed GPS minus that predicted due to viscoelastic relaxation) to develop combined viscoelastic relaxation and afterslip models. We are able to find a mechanical model that fully explains all observed geodetic on-land and seafloor horizontal and vertical postseismic displacements. We find that postseismic displacements are in about equal parts due to viscoelastic relaxation and afterslip, but their patterns are spatially distinct. Accurately predicting both horizontal and vertical on-land postseismic displacements requires a mantle wedge viscosity structure that is depth dependent, reflecting the manner in which temperature, pressure, and water content influence viscosity. No lateral heterogeneities within the mantle wedge viscosity structure beneath northern Honshu are required. Westward-directed postseismic seafloor displacements may be due flow via low-temperature, plastic creep within the lower half of a Pacific lithosphere weakened by plate bending. The distribution of afterslip is controlled by the location of coseismic slip from the Tohoku-oki and other regional historic earthquakes. The paradigm by which afterslip is thought of as the dominant postseismic mechanism immediately following earthquakes, with viscoelastic relaxation to follow in later years, is shown to no longer be valid.

1. Introduction

While the net effect of earthquakes is to release the stress that is built up on faults by the steady motion of tectonic plates, earthquakes cause an increase in stress in regions surrounding the area of fault slip. Rheologically weak regions within the lower crust and mantle that cannot sustain these stresses will flow due to viscoelastic relaxation, or in the case of weak regions on a fault, may slip aseismically, as "afterslip". Both processes cause postseismic surface displacements (e.g., Bürgmann and Dresen, 2008) as recorded by Global Position System (GPS) or other geodetic means which can be used to constrain viscoelastic structure and regions of afterslip.

The 2011 M9 Tohoku-oki megathrust earthquake offers a unique opportunity for postseismic analysis of subduction zone rheology. More than 800 continuous GPS stations located throughout northern Japan are recording displacements in high spatial density and, for the first time, an array of seafloor geodetic measurements extends coverage offshore (Fig. 1). These observations provide a chance at solving a challenging problem facing all postseismic studies: how does one uniquely determine the relative contributions of viscoelastic relaxation versus afterslip. Any proposed solution must accurately account for both observed horizontal and vertical postseismic displacements. Both deformation patterns are critical because viscoelastic relaxation occurring at various depths, as well as afterslip, tend to cause similar postseis-

* Corresponding author.
E-mail address: freed@purdue.edu (A.M. Freed).
[1] Present address.

http://dx.doi.org/10.1016/j.epsl.2016.11.040
0012-821X/

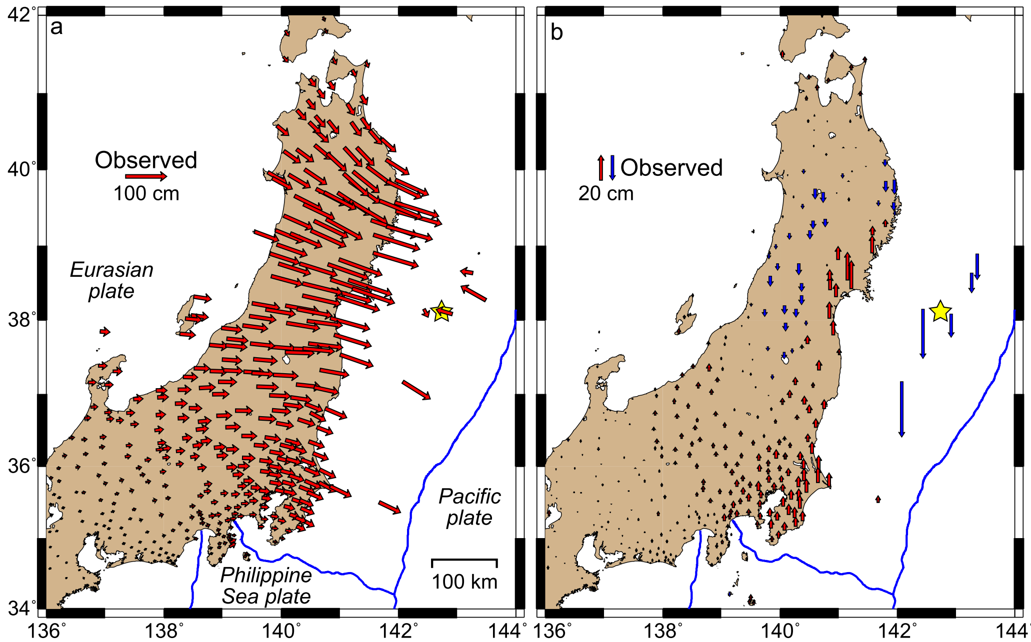

Fig. 1. Cumulative, three year (a) horizontal and (b) vertical observed postseismic displacements based on analytical fits (see text) to the GPS time-series. Blue lines denote plate boundaries. Yellow star indicates epicenter of the Tohoku-oki earthquake.

mic horizontal displacements (e.g., Wang et al., 2012). However, vertical postseismic deformation will often flip sign from uplift to subsidence depending on the depth of flow or slip (e.g., Freed et al., 2006, 2007). In most postseismic analyses, the lack of dense geodetic coverage, and greater inherent errors in GPS vertical displacements, limits the degree to which the relative contributions of viscoelastic relaxation and afterslip can be resolved. This is particularly problematic following subduction zone earthquakes, where geodetic measurements are generally limited to a few dozen GPS stations confined to the on-land side (e.g. Lin et al., 2013; Wiseman et al., 2015).

The coverage following the Tohoku-oki earthquake overcomes most of these issues. Particularly, the vertical deformation pattern is clearly imaged on land (Fig. 1b). Yet, no postseismic studies to date have comprehensively explored both horizontal and vertical postseismic displacements following the M9. Either such studies do not show how vertical surface deformation from models compares to observations (Diao et al., 2014; Sun et al., 2014, 2015), or the comparison shows systematic errors (Perfettini and Avouac, 2014; Shirzaei et al., 2014; Yamagiwa et al., 2015; Hu et al., 2014, 2016). All of these previous studies considered a combination of viscoelastic relaxation and afterslip to explain postseismic displacements following the Tohoku-oki earthquake (except for Perfettini and Avouac, 2014, which was purely afterslip). Given that afterslip fits are based on inversions for a large number of slip combinations on numerous fault patches, it is perhaps surprising that the vertical postseismic observations could not be better matched with such models. This suggests that the density of the Japan GPS array is such that only an accurate combination of viscoelastic and afterslip assumptions can explain the data.

The objectives of our study are to determine the relative contributions of viscoelastic flow and afterslip to cumulative postseismic horizontal and vertical displacements following the 2011 Tohoku-oki earthquake, and to find the viscosity structure responsible for the displacements. There are two main approaches to inferring the distribution of afterslip following an earthquake. Many previous studies of afterslip following the Tohoku-oki earthquake used observed postseismic displacements to directly invert for afterslip (e.g., Ozawa et al., 2012; Diao et al., 2014; Perfettini and Avouac, 2014; Yamagiwa et al., 2015). This approach has the advantage of solving for the afterslip distribution that best explains postseismic observations. However, it provides no physical insight into the processes, e.g., the role of friction, fault geometry, the prestress state, and coseismic stress changes on the afterslip distribution. Several studies have thus considered stress-driven afterslip following the Tohoku earthquake to provide more insight (e.g., Hu et al., 2014), even utilizing information from small repeating earthquakes to improve constraints on slip behavior (Hu et al., 2016). This approach, however, is at the expense of a more precise agreement between calculated and observed postseismic displacements.

Similarly, there are different approaches to how one models viscoelastic relaxation. Many of the previous Tohoku-oki postseismic analyses attempted to fit GPS displacement time-series, usually by assuming a biviscous Burgers rheology, where an initial short term viscosity is assumed to transition into a longer term viscosity (e.g., Pollitz, 2003; Sun et al., 2014). However, without first understanding the relative contributions of viscoelastic relaxation and afterslip, such approaches provide limited information regarding the structure of either mechanism. In addition, a biviscous rheology is mainly a convenient means to explain displacement rate-changes associated with a transient rheology. In terms of the underlying physics, the data may be more likely due to a continuous increase of effective viscosities due to stress-dependent rheologies (e.g., Freed and Bürgmann, 2004).

Previous analyses of postseismic relaxation have used simplifying approximations, including a depth-invariant viscosity structure for the mantle wedge (Diao et al., 2014; Hu et al., 2014, 2016), and an *a priori* uniform viscosity for the wedge and oceanic mantle based on inferences from other subduction zone studies (Sun et al., 2014, 2015; Shirzaei et al., 2014; Yamagiwa et al., 2015). This in light of viscosity likely being dependent on temperature, pressure, and water content (e.g., Hirth and Kohlstedt, 2003; Freed et al., 2011), and therefore highly depth-dependent, as well as likely to vary from subduction zone to subduction zone.

A second potential problem in several previous postseismic studies is the incorporation of a coseismic slip distribution from a separate study, often from a model with a different methodol-

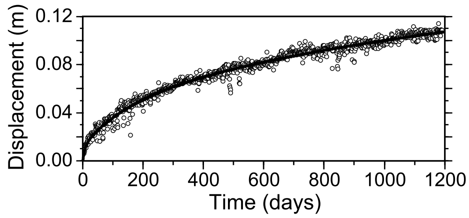

Fig. 2. Comparison of total horizontal displacement GPS daily solutions (dots) for station 92106 (latitude 35°, longitude 103.9°) and a functional representation of the data (line) using equation (2) with relaxation times of 9, 154, and 1514 days.

ogy without verification of the coseismic displacements (e.g., Diao et al., 2014; Hu et al., 2014, 2016; Sun et al., 2014, 2015). While the surrounding region can dampen how errors in the coseismic slip propagate into postseismic results, a match to coseismic displacements should exist to insure that the overall coseismic slip distribution are consistent with the postseismic deformation. This may not be the case when two different elastic structures are assumed (e.g., Hearn and Bürgmann, 2005).

We surmise that the aforementioned over-simplifications are in part the reason why previous postseismic studies have had a difficult time to explain both horizontal and vertical postseismic displacements following the Tohoku-oki earthquake. Here, we develop a model that considers a strongly layered crustal and mantle rheology and a seismically guided 3-D structure of the region including the influence of the subducting Philippine Sea Plate (ignored by earlier studies). We use the model to calculate postseismic surface displacements due to a variety of rheologies and to invert for afterslip based on residual displacements (observed minus that due to viscoelastic relaxation). We explore a large range of parameter space in search of combined viscoelastic and afterslip displacements that agree with both the horizontal and vertical postseismic displacements.

2. Geodetic constraints

Land-based postseismic displacements following the 2011 Tohoku-oki earthquake are based on daily location solutions for more than 1200 continuous GPS stations (GEONET) processed by the Geospatial Information Authority of Japan (GSI) (Ozawa et al., 2012). Time-series after January 1 1998 were provided by GSI. We removed annual and semiannual trends estimated from the period between January 1 2006 and December 31 2008. Then, pre-earthquake (secular) velocities are estimated from the stable period between January 1 1998 and December 31 1998 and removed. We used 766 time-series which include data in the periods between January 1 2006 and December 31 2008, period between January 1 1998 and December 31 1998, and the period after March 11 2011. In order to minimize non-tectonic components in remaining postseismic transients, we fit each time-series with an asymptotic relaxation process of the form

$$f(t) = a\Big(1 - d\exp(-t/b_1) - c\exp(-t/b_2) - (1-c-d)\exp(-t/b_3)\Big), \tag{1}$$

where a is overall amplitude, c and d partition the contribution of different decay times, and b_i are relaxation times (Fig. 2). Typical 3-year times-series are well described by a combination of ∼10-, ∼150-, and ∼1500-day relaxation times, although we note that absolute values for the b_i depend on the time series length. This fit enables us to determine cumulative displacements at any given time period. The dense GPS array enables patterns in cumulative vertical postseismic displacements to be readily visible (Fig. 1b), minimizing the influence of non-tectonic processes and noise that often accompanies such data. The verticals show widespread onshore uplift except for two regions, which show prominent subsidence. One is along the western half of northern Honshu, coincident with the volcanic arc, and the second is along the northeast coast.

We also utilized 3-year postseismic displacements at six seafloor GPS-acoustic (GPS-A) stations that were surveyed by the Japanese Coast Guard (Watanabe et al., 2014) and one GPS-A station by Tohoku University (Sun et al., 2014) (Fig. 1). Note that only horizontal displacements were obtained at the station of Tohoku University. We removed the approximately 8 cm/yr interseismic velocity along the edge of North American Plate margin associated with subduction of the Pacific Plate (Sella et al., 2002; Apel et al., 2006). While all of the onland postseismic, horizontal GPS displacements are toward the east, as one would be expect from either viscoelastic relaxation or afterslip (Wang et al., 2012), several seafloor displacements are toward the west (Fig. 1a). Horizontal postseismic displacements directed away from the trench following a subduction zone earthquake have never before been observed. As discussed below, such displacements imply viscoelastic relaxation within relatively shallow oceanic mantle, in contrast to previous postseismic studies of subduction zones where oceanic asthenosphere is generally found to be an order of magnitude higher viscosity than that of a presumably wetter mantle wedge (e.g., Hirth and Kohlstedt, 2003). Sun et al. (2014) suggest that westward-directed seafloor displacements may be due to a thin, viscously weak layer at the base of the oceanic lithosphere, an idea we test here along with an alternate hypothesis of plastic weakening within the lithosphere.

3. Modeling approach

We developed a 3-D finite element model using the software *ABAQUS* (www.3ds.com). Our mesh incorporates the geometry associated with the Pacific and Philippine Sea Plate slabs based on the distribution of interplate earthquakes (Baba et al., 2002; Nakajima and Hasegawa, 2006, 2007; Hirose et al., 2008a, 2008b; Nakajima et al., 2009; Kita et al., 2010; Hayes et al., 2012) (Fig. 3). The model extends more than 1000 km in all horizontal directions from the Tohoku-oki epicenter and to a depth of 600 km. Model side and bottom boundaries are held fixed. We tested the influence of these boundary conditions and found the effect to not significantly influence model results. We also incorporate a 3-D elastic structure based on inferred seismic velocities (e.g., Matsubara et al., 2008; Nakajima et al., 2009). The elastic structure assumed in the model is shown in Fig. 3 inset (the oceanic elastic structure subducts with the slab). All materials assume a Poisson's ratio of 0.25.

Coseismic slip is applied as constraint equations that specify an instantaneous slip along a predefined fault surface divided into a set of patches. We solve for Green's functions that relate surface displacements associated with slip on each patch, then invert for the distribution of slip that best explains observed displacements given roughness damping as determined from misfit-roughness tradeoff analysis. We assumed equal weighting of horizontal and vertical displacements at all stations. This is equivalent to setting a lower weighting on coseismic seafloor displacements simply because there are far fewer compared to on-land measurements. Though it is difficult to assess the uncertainty of the seafloor measurements, they are almost certainly less accurate than those on land, and this approach reflects that realization.

Fig. 4 shows the inferred slip distribution and a comparison of observed and predicted coseismic displacements. Numerous coseismic slip solutions have been previously published with a wide range of slip distributions and maximum slip levels due to a wide range of modeling assumptions and observational constraints (see

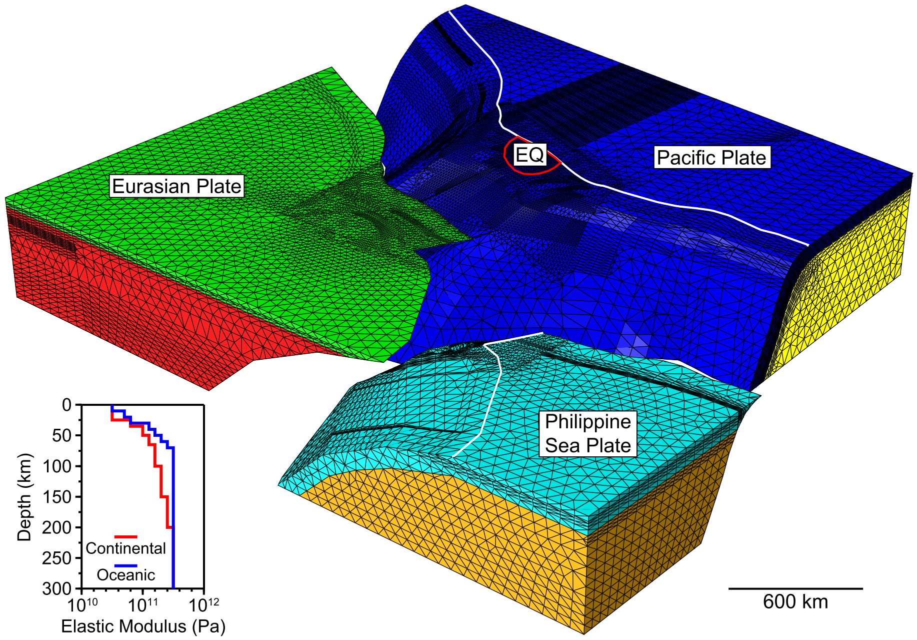

Fig. 3. Finite element mesh used with the major components separated to reveal the internal structure. Color changes with depth illuminate approximate lithosphere/asthenosphere boundaries. The region encompassing coseismic slip greater than 3 m is labeled "EQ". Inset shows the assumed elastic structure (Young's modulus).

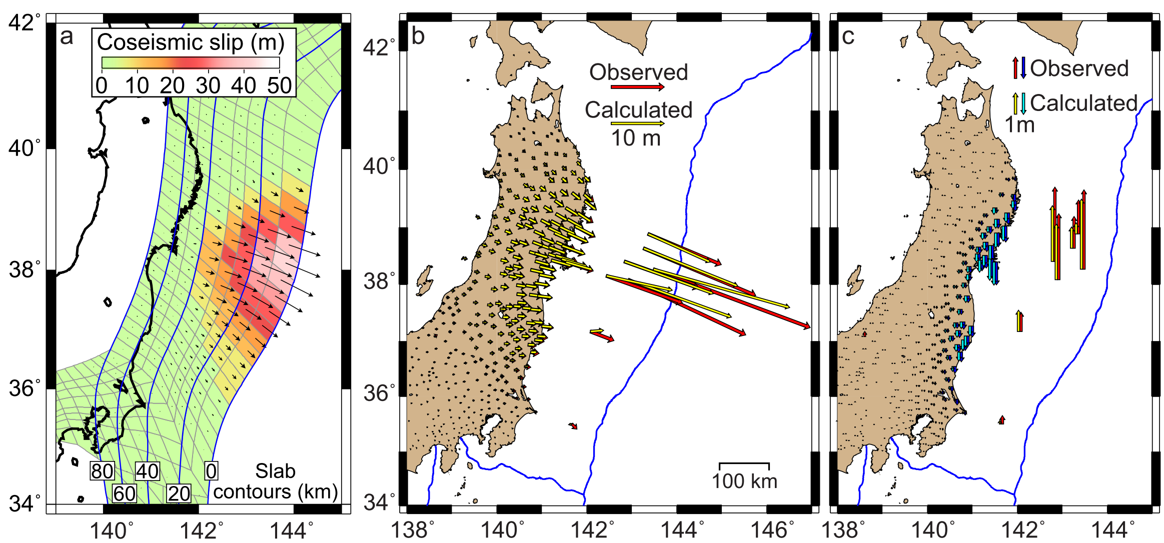

Fig. 4. (a) Inferred coseismic slip based on an inversion of the observed coseismic surface displacements utilizing elastic Green's function based on the finite element model. Comparison of observed and calculated horizontal (b) and vertical (c) coseismic displacements.

review by Tajima et al., 2013). Our maximum inferred slip of ∼45 m is in the middle of the 30–60 m range for the maximum slip inferred by most of these models (Tajima et al., 2013). Moreover, our inferred slip distribution is similar to that inferred by many previous studies in the manner in which slip is greatest at the trench and decays with depth (e.g., Yamazaki et al., 2011; Iinuma et al., 2012; Kyriakopoulos et al., 2013; and Pulvirenti et al., 2014). Our coseismic model displacements are in excellent agreement with all land-based measurements, with, as expected, larger misfit for the seafloor measurements. We could have achieved a more accurate fit to the seafloor displacements by reducing the smoothness of the inferred slip distribution, but did not believe such a solution was warranted given the uncertainty in seafloor measurements. Notably, alternate slip distributions with the same basic pattern of slip and seismic moment did not significantly influence our postseismic results. This is because strong lithosphere surrounding the plate interface acts as a filter that smooths stress changes associated with refined structure within the slip distribution.

Because we are only interested in matching 3-year, cumulative postseismic displacements in this study, displacement rate-changes are expected to not play a major role, and we therefore use an effective, Newtonian Maxwell rheology. For each candidate viscosity structure, we apply coseismic slip to the model, and then allow coseismic stresses to relax for 3 years. For combined viscoelastic relaxation and afterslip models, we first solve for the residual surface displacements (observed minus displacements from viscoelastic relaxation), and then invert for afterslip. Afterslip inversions utilize the same Green's functions calculated for the coseismic inversion, with fault slip enabled to a depth of 80 km.

We test various models against the observed 3-yr cumulative displacements using the sum of squared residuals (*ssr*) given by:

$$ssr = \sqrt{(1/n)\sum(x_o - x_m)^2} \quad (2)$$

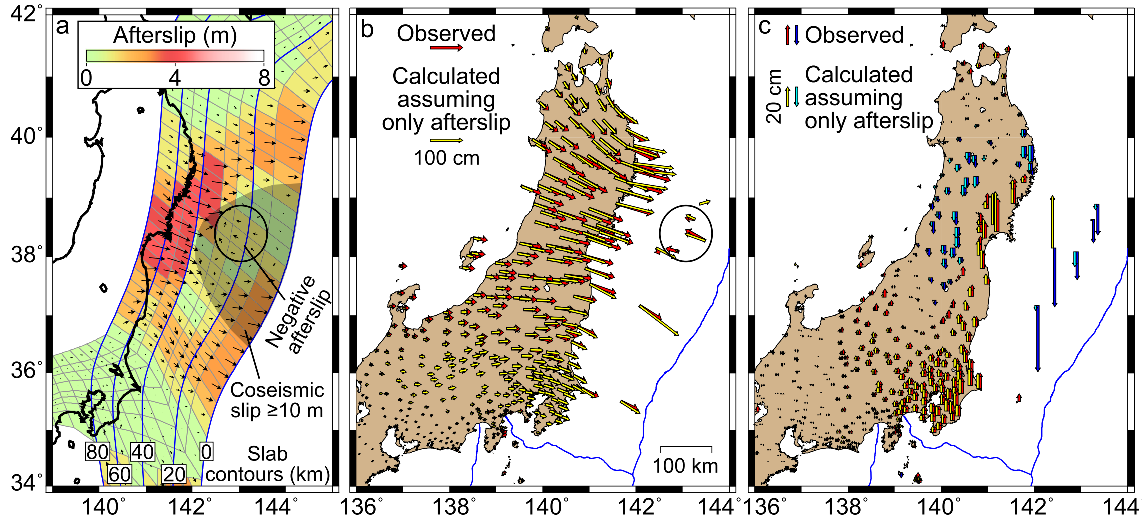

Fig. 5. (a) Inferred afterslip slip based on an inversion of the observed 3-year cumulative postseismic surface displacements utilizing elastic Green's functions. Comparison of observed and calculated horizontal (b) and vertical (c) cumulative displacements. Circles in (a) and (b) denote region where afterslip must be negative (slip associated with extension on the plate interface) in order to explain westward directed postseismic displacements.

Table 1
Description and misfit of sample models discussed in text.

Model number	Category	Description	On-land horizontal misfit	On-land vertical misfit	Offshore (total)
1	Afterslip only	Afterslip only with uniform weighting[1] of 1/1/1	1.9	1.3	73
2	Afterslip only	Afterslip only with weighting of 3/1/1	1.1	10.1	200
3	Afterslip only	Afterslip only with weighting of 1/1/3	5.2	24	12
4	Viscoelastic (VE) only	Best-fitting VE only (Fig. 7a, no afterslip)	8.0	2.4	100
5	Combined[2]	VE Model 4	1.1	1.7	10
6	Combined	VE Model 4 with weak oceanic sublithospheric layer	1.1	1.8	12
7	Combined	VE Model 4 without a cold nose	4.8	9.0	35
8	Combined	VE Model 4 with cold nose extended 50 km to the west	1.2	2.0	10
9	Combined	VE Model 4 below a 35 km thick lithosphere	1.2	1.8	12
10	Combined	VE Model 4 below a 50 km thick lithosphere	1.3	2.1	16
11	Combined	Uniform mantle wedge viscosities below a 35 km thick lithosphere	2.0	4.6	10
12	Combined	Uniform mantle wedge viscosities below a 50 km thick lithosphere	1.4	2.9	13
13	Combined	VE Model 4 with mantle wedge viscosities increased by 20%	1.0	1.6	14
14	Combined	VE Model 4 with mantle wedge viscosities increased by 40%	1.1	2.5	29
15	Combined	Model 5 with afterslip inversion weighting of 1/3/1	1.3	1.1	14
16	Combined	Model 5 with afterslip inversion weighting of 1/3/3	1.4	1.2	2.7
17	Combined	Model 5 with afterslip inversion weighting of 1/3/10	1.8	1.3	1.0
18 (preferred)	Combined	Model 12 with afterslip inversion weighting of 1/3/1	1.2	1.0	16
19	**Combined**	**Model 12 with afterslip inversion weighting of 1/3/3**	**1.2**	**1.1**	**3.0**
20	Combined	Model 12 with afterslip inversion weighting of 1/3/10	1.6	1.2	1.0

Notes:
[1] Unless otherwise state, afterslip inversions are based on a uniform weighting of on-land residual horizontal displacements, on-land residual vertical displacements, and offshore displacements of 1/1/1, respectively.
[2] Combined models calculated postseismic displacements based on an assumed viscoelastic rheology, then invert for afterslip based on the residual (observed minus postseismic displacements).

where n is the total number of observations (3 components per station) and x_o and x_m are the observed and modeled surface displacements. In consideration of the density of the GPS array, and because we use analytical fits that smooth out noisy time-series data, we assume uniform observational errors and thus do not weight individual station data by their uncertainty.

To determine the most appropriate viscoelastic models we utilize as a second criteria that on-land horizontal postseismic displacements (all directed easterly) cannot exceed those observed. This is because postseismic displacements associated with afterslip are only able to contribute an easterly directed displacement without violating the assumption that subduction zone interfaces only slip in a thrusting manner (we do not expect normal faulting to occur along a megathrust). Therefore, over-predicted viscoelastic displacements cannot be countered by afterslip when the two models are combined.

4. Results

4.1. Full afterslip inversion

We initially assume that all of the postseismic data is due to afterslip (referred to here as the *full afterslip* inversion) and invert for the slip required to explain the cumulative displacements. Fig. 5 shows the inferred afterslip distribution and a comparison of the observed and predicted surface displacements based on equal weighting of all on-land horizontal, on-land vertical, and offshore displacements (denoted as 1/1/1, respectively). Compared to the best combined viscoelastic relaxation and afterslip solutions described below, this solution leads to almost twice the misfit of on-land horizontal displacements, ~30% greater misfit of on-land vertical displacements, and a misfit ~73 times greater than for offshore postseismic displacements (see Model 1 in Table 1).

The poor fit to the horizontal on-land data is primarily due to an underprediction, by as much as 50%, in the latitudes that span the central region of the coseismic displacements (37°N–39°N in Fig. 5b). This fit can be improved by increasing the weighting of these displacements in the inversion, but at great cost to the already mediocre fit to the onshore vertical displacements (see Model 2 in Table 1). Any attempt to improve the fit to seafloor data comes at great expense to the fit to on-land displacements (see Model 3 in Table 1). Thus, despite a significant number of degrees of freedom, a satisfactory solution to the observed cumulative postseismic displacements cannot be achieved by attributing all postseismic displacements to afterslip, as seen in Perfettini and Avouac (2014).

In addition to the misfit issues, the full afterslip inversion has a plausibility issue in that it requires slip in the opposite sense (circle in Fig. 5a) expected of a megathrust in order to explain westward directed seafloor displacements (circle in Fig. 5b) as noted by Sun et al. (2014). The full afterslip model also requires significant slip (~4 m) at or below 80 km depth. This becomes problematic to explain as afterslip, since the mantle wedge/slab interface is fairly hot (>400 °C) at this depth (e.g., Fig. 2a in Peacock and Wang, 1999) and thus unlikely to sustain a narrow shear zone. Inferred deep slip is more likely due to viscoelastic flow with the mantle wedge, as we discuss below. The best fit of the full afterslip model to postseismic displacements occurs to the north and south of the coseismic slip region. These displacements are primarily driven by shallow (<40 km depth) slip off of the northern and southern shores.

4.2. Viscoelastic relaxation models

We next determine the best pure viscoelastic relaxation model. Our exploration of model space considers a set of model parameters typical of previous subduction zone postseismic studies, such as the viscosity of a uniform mantle wedge and oceanic mantle. We also consider additional parameters, such as a depth-dependent mantle wedge viscosity structure and the lateral extent of the cold "nose", the corner of the mantle wedge where cold temperatures prevail due to the close proximity of both the upper plate and slab (e.g., Syracuse et al., 2010). These factors are generally not considered because of the typical lack of sufficient observational constraints following subduction zone earthquakes. However, the density of the Japan GPS network is sufficient so as to be sensitive to these factors. This dense coverage also enables us to explore model parameters such as the depth extent of the Philippine Sea Plate, which extends into the southern region of the postseismic response.

Parameter space would ideally be explored with an analysis of all possible combinations of reasonable ranges of the model parameters. However, the number of parameters combined with the run time of each model (several hours) is beyond our computer resources. We thus utilize a guided trial and error approach where we explore model space associated with a viscoelastic relaxation-only scenario in several phases. In the first phase, starting from an initial estimate of model parameters based on previous studies (e.g., a mantle wedge with a uniform viscosity of 10^{19} Pa s and an oceanic mantle with a viscosity of 10^{20} Pa s; e.g. Wang et al., 2012; Hu et al., 2014), we systematically march through a range of each model parameter to arrive at an initial combination that provides minimum misfit (Fig. 6). Misfit is based on the *ssr* misfit of all on-land and offshore horizontal and vertical GPS displacements, and is normalized to the misfit of the best-fitting combined (viscoelastic relaxation and afterslip) model discussed below.

In a second phase, we then repeat the process starting with the best-fitting model from the first phase. This step is required because of trade-offs between model parameters that will lead to different solutions based on the order in which the parameters are varied. Every time we find a reduction of misfit from a change in a model parameter we then return to the other parameters to see if further reductions in the misfit can be achieved. In this fine-tuning phase we not only find the depth of the lowest viscosity layer in the mantle wedge and oceanic mantle, for example, but also adjust each layer above and below to find the best-fitting, depth-dependent structure. The result of this second phase is our best-fitting viscoelastic relaxation-only model shown in Fig. 7. This approach does not necessarily guarantee that we have found the global minimum misfit model. But nor does the global minimum misfit model guarantee that one has found the correct model. To this end, we examine the plausibility of the inferred viscoelastic structure (discussed below).

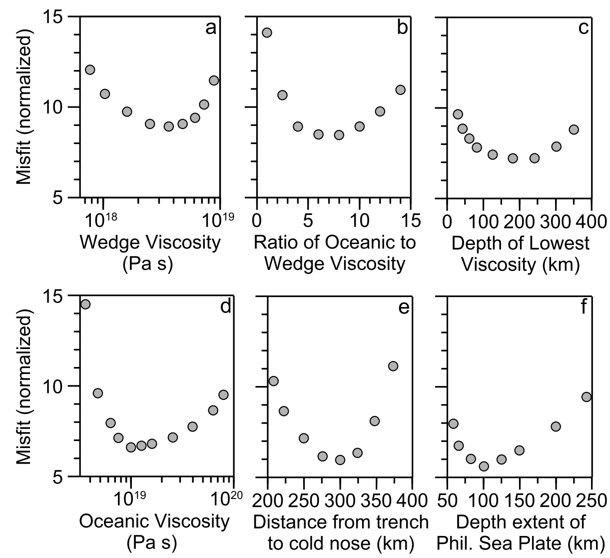

Fig. 6. Misfit of viscoelastic relaxation only models as a function of (a) the viscosity of a uniform mantle wedge, (b) the ratio of the viscosity of a uniform oceanic asthenosphere with respect to the viscosity of a uniform mantle wedge, (c) the depth of the lowest viscosity within a non-uniform mantle wedge, (d) the viscosity of a uniform oceanic asthenosphere when combined with the best-fitting non-uniform wedge viscosity structure, (e) the distance from the trench to the western edge of the mantle wedge cold nose (the location where viscoelastic flow in the corner of the wedge is weak enough to flow), and (f) the depth extent of the Philippine Sea Plate subducting slab. Misfits have been normalized to the best-fitting combined (viscoelastic relaxation plus afterslip) model described in Table 1.

Our best-fitting viscoelastic relaxation-only model results in the overall pattern of horizontal and vertical postseismic displacements shown in Figs. 7b and 7c. Viscoelastic relaxation causes postseismic displacements in the center of the larger observed displacement field, and shows flow towards the region of coseismic displacement (gray region in Fig. 7b). Viscoelastic relaxation cannot explain the broader pattern of postseismic displacements (to the north and south), as shown in the residual horizontal displacements (Fig. 7d). There are no adjustments to the viscosity structure that can broaden the influence of viscoelastic relaxation into these northern and southern regions, arguing for the importance of afterslip in these regions.

Our inferred viscosity structure (Fig. 7a) has a modestly weak lower crust (25–35 km depth) from which the viscosity structure weakens steadily with depth to 150 km. Below 300 km, the viscosity begins to increase again, with a more significant jump at 400 km depth, the approximate depth of the olivine to spinel transition. This inferred viscosity structure was strongly influenced by the pattern of the observed vertical displacements, which transitions from uplift along the east coast to subsidence along the west coast (Fig. 7b). Relaxation at depths above 100 km tend to cause subsidence at the surface, while deeper relaxation causes uplift.

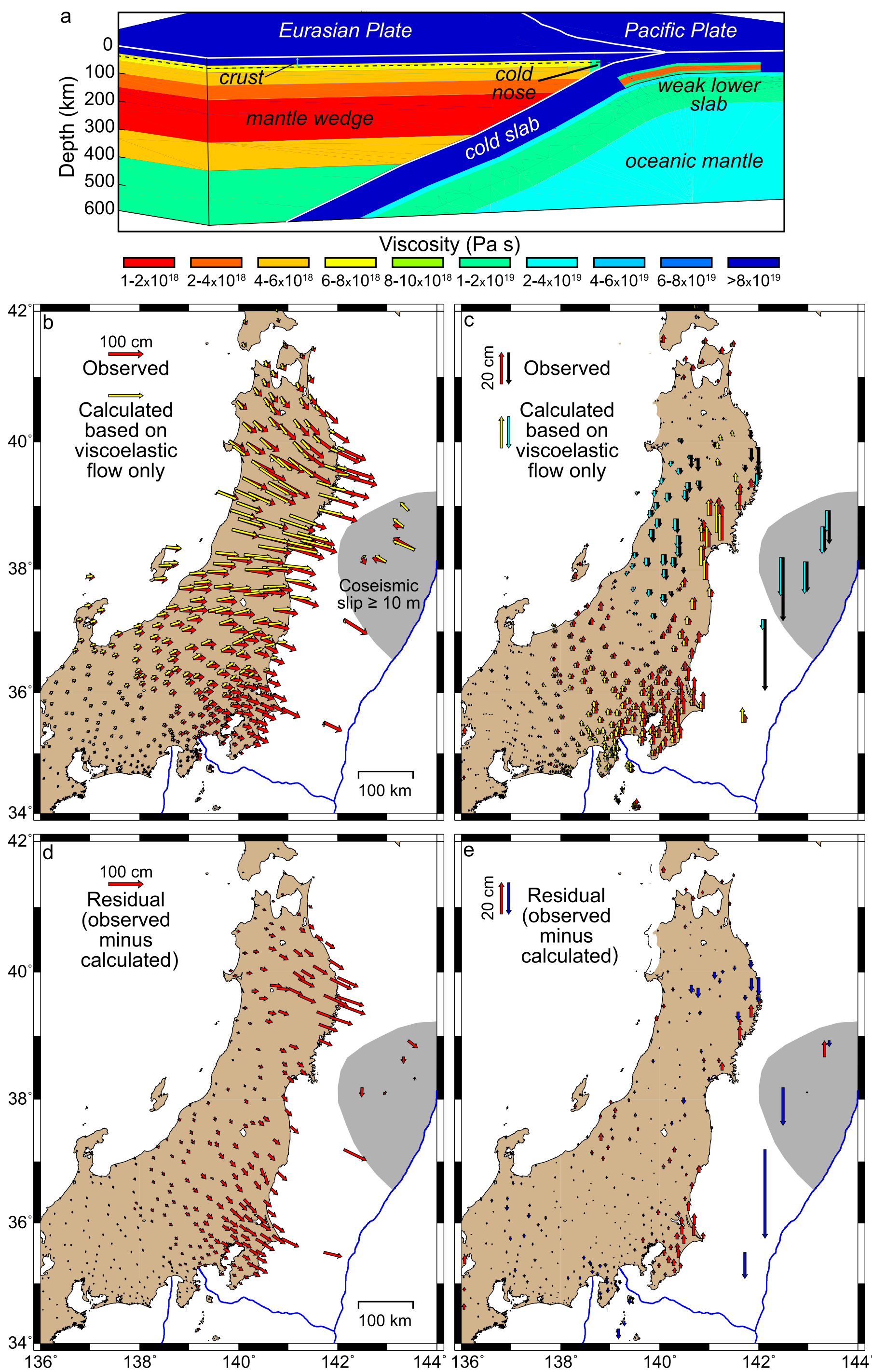

Fig. 7. (a) Viscoelastic structure for the best-fitting viscoelastic relaxation only model (no afterslip). Comparison between observed and calculated horizontal (b) and vertical (c), 3-yr cumulative postseismic displacements. Residual displacements (observed minus calculated) are shown in (d) and (e) for horizontal and vertical displacements, respectively.

The observed pattern is thus explained by the 100 km depth of the Pacific slab as it subducts beneath the Japan coast.

Our best-fitting model has a cold nose extending to ∼200 km from the trench, with the western-most 50 km modeled with an intermediate viscosity suggesting a transition from a strong to a weak rheology.

The depth extent of the Philippine Sea Plate slab influences the southern region of the postseismic deformation field, with the depth extent of the plate into the mantle strongly influencing the magnitude of calculated displacements in this region—the deeper the extent of the slab, the more muted the postseismic response in this region. This influence enabled us to infer that the Philippine Sea Plate extends to ∼100 km depth, with the viscosity below 60 km requiring an intermediate viscosity compared to the surrounding mantle. This is consistent with the observed seismic structure indicating that the Philippine Sea Plate terminates between 90 and 200 km depth (Nakajima et al., 2009).

Sun et al. (2014) explained the westward seafloor displacements as resulting from a thin (10 km thick) low viscosity (2×10^{17} Pa s) channel at the base of the lithosphere (80–90 km depth) that terminates at ∼250 km depth as it subducts beneath Japan. However, Sun et al. (2014) did not attempt to match vertical dis-

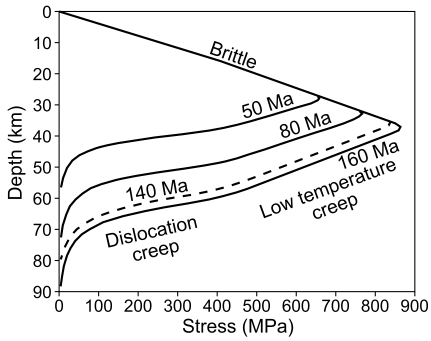

Fig. 8. Deformation-limited stress in the lithosphere due to bending at a subduction zone as a function of lithospheric age (modified from Buffett and Becker, 2012). The maximum stress coincides with a transition between brittle failure (above) and creep (below), with creep transitioning from low-temperature (Peierls) plasticity to higher temperature dislocation creep.

placements. We find that a thin-low viscosity channel can only extend to ∼100 km depth without adverse effects on the goodness of fit of on-land vertical displacements. Thus, we refine the suggestion that westward seafloor postseismic displacements are caused by relaxation of a low viscosity channel as the base of the lithosphere by limiting its extent to not pass below the Pacific coast of northern Honshu.

We explore an alternate hypothesis to westward directed seafloor displacements; that it is occurring within the lower part of the Pacific slab (lithosphere) itself. A thermo-mechanical analysis by Buffett and Becker (2012) explores where the bending of subducting slabs should lead to failure of the lower lithosphere in the form of plastic flow—low temperature Peierls-creep in the mid-lithosphere and dislocation creep in the lower lithosphere (Fig. 8). If a subducting slab is already experiencing failure level stresses at the trench, then any additional stress, such as that from a large earthquake, should exceed yield stress levels and thus induce viscoelastic flow to return stresses back to the yield level. For the age of the Pacific slab where it subducts beneath northern Honshu (∼140 Myr), the onset of plastic deformation should occur at ∼40 km depth (dashed curve in Fig. 8; Buffett and Becker, 2012).

We allow the viscoelastic model to relax in the bottom half of the Pacific slab (40–80 km depth), in a region that extends 200 km westward down dip from the trench and 300 km eastward out into the surface portion of the plate (Fig. 7a), the general range of plate bending. We explore several possible viscosity structures within the lower slab, settling on a best-fitting one in which the viscosity is a minimum of 3×10^{18} Pa s between 50 and 70 km depth (Fig. 7a). The goodness of the fit of the westerly directed seafloor horizontal displacements is shown in Figs. 7b and 7d.

4.3. Combined viscoelastic and afterslip models

Here, we use the residual displacements (observed minus viscoelastic relaxation) to invert for afterslip (referred to here as *residual afterslip*). Starting with the best-fitting viscoelastic only model (Fig. 7a), we invert for afterslip using an equal 1/1/1 weighting scheme. The resulting misfit (model 5 in Table 1) for the combined model represents a significant improvement over the best full-afterslip model. However, modest misfit remains with the on-land vertical displacements and the offshore displacements. In the same fashion that full afterslip inversion could not fully explain postseismic displacements despite the great number of degrees of freedom, it may be difficult for residual afterslip to satisfy remaining misfit if the viscoelastic model is not close enough to the correct viscosity structure.

We explored a number of alternate viscoelastic structures, each a perturbation on the best-fitting viscoelastic relaxation only model. We begin by exploring whether the westward seafloor displacements can be equally well explained by a 10-km-thin, viscously weak, oceanic sublithospheric layer instead of a weak lower lithosphere due to bending stresses. We find that this model combined with its associated residual afterslip provides almost as good a solution (model 6 in Table 1). We next explore whether the assumed extent of the cold nose is the best choice, varying it from no nose (model 7 in Table 1) to a nose extending another 50 km to the west (model 8). We find that any change to the extent of the cold nose leads to an increase in misfit. We consider an elastic lower crust (model 9) and a strong lithosphere to a depth of 50 km (model 10), both of which lead to greater misfit. We also consider models with a uniform viscosity within the mantle wedge beneath a 35 and 50 km-thick lithosphere (models 11 and 12, respectively). These viscosity structures, combined with their associated residual afterslip, lead to significantly greater misfit.

Next, we take the best-fitting viscoelastic relaxation only structure (Fig. 7a) and uniformly increase the absolute mantle wedge viscosity (preserving the relative viscosity of the layers). This has the effect of decreasing the contribution of viscoelastic relaxation and increasing afterslip. We increased mantle wedge viscosities from 10 to 50%. Table 1 highlights the case of a 20% (model 13, Fig. 9a) and a 40% viscosity increase (model 14). The 20% viscosity increase model lead to the best-fitting combined model for the 1/1/1 inversion weighting. We then considered alternate weightings in the inversions for residual displacements. Models 15–20 in

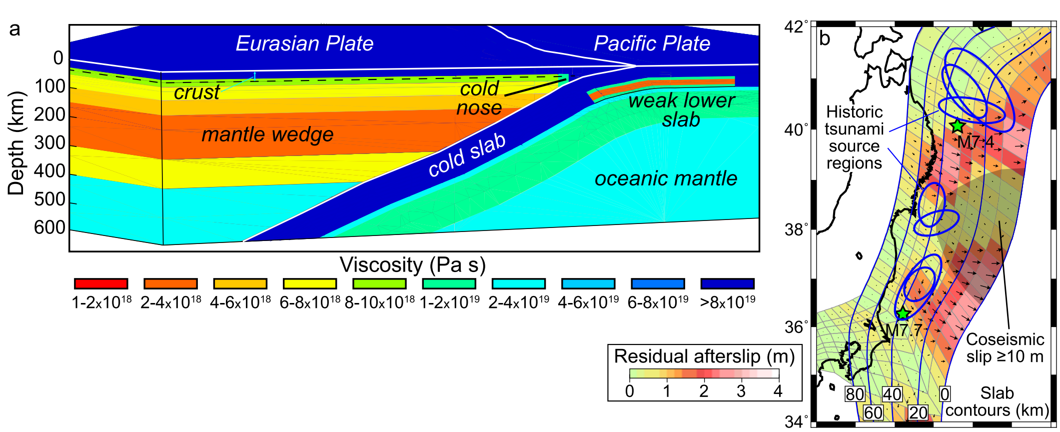

Fig. 9. (a) Viscoelastic structure and (b) afterslip that together provide the best-fitting explanation of the 3-yr observed postseismic displacements following the 2011 Tohoku-oki earthquake. The green stars are the epicenters of the two largest interplate aftershocks following the Tohoku-oki earthquake (Nishimura et al., 2011). Tsunami source regions denoted by blue ellipses are from Hashimoto et al. (2009).

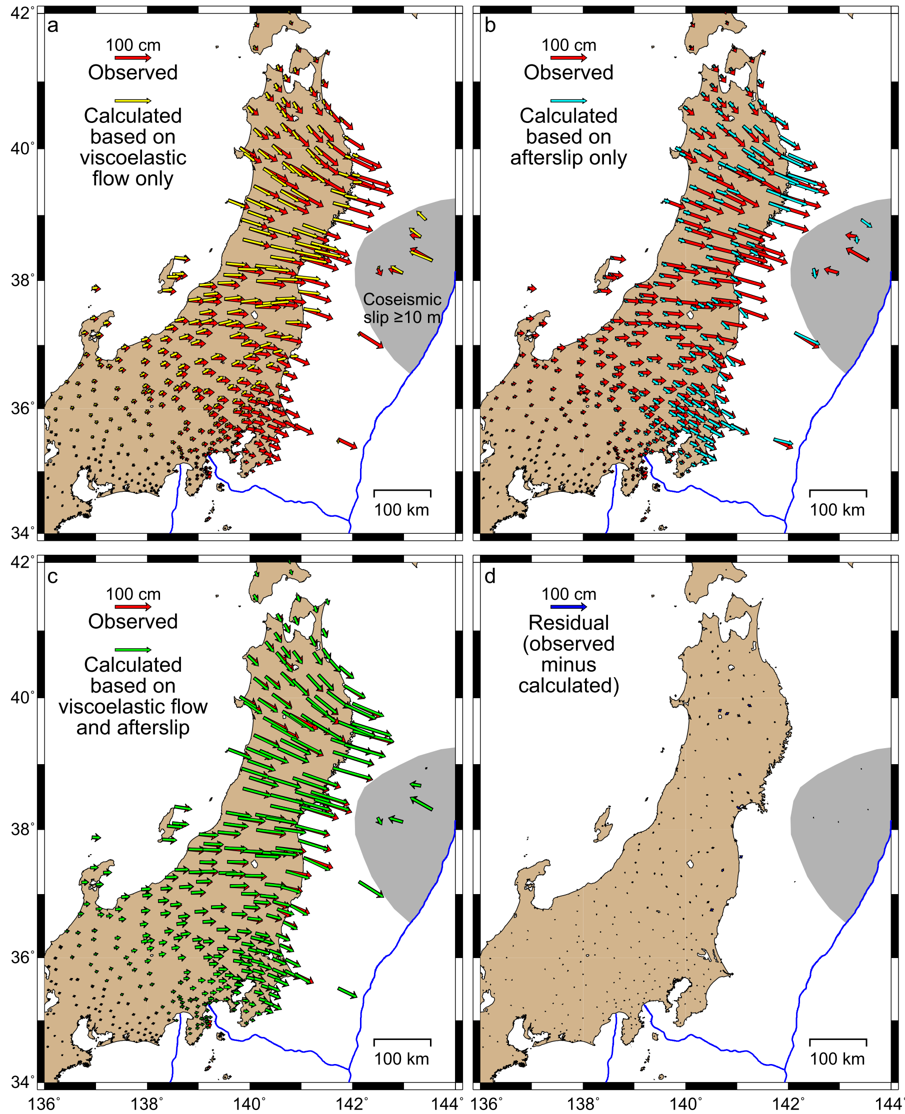

Fig. 10. Comparison of calculated and observed horizontal displacements associated with (a) viscoelastic relaxation (viscosity structure shown in Fig. 9a) and (b) afterslip (afterslip distribution shown in Fig. 9b) associated with the best-fitting combined model (model 19 in Table 1). (c) Horizontal displacements associated with the combined contributions viscoelastic relaxation and afterslip for the best-fitting model, and (d) associated residual horizontal displacements (observed minus combined calculated displacements).

Table 1 highlight some of the weightings of various models we considered. A weighting of 1/3/3 using the viscoelastic model that considered a 20% increase viscosity (Fig. 9a), provides the best all-around fit to the observed postseismic data (model 19 in Table 1). We choose model 19 as the best-fitting model despite greater misfit to the offshore data compared to other models due to the fact that the uncertainty of this data is likely highest. The afterslip associated with model 19 is shown in Fig. 9b. It contains up to $\sim$3 m of afterslip mostly surrounding the region where coseismic slip was at least 10 m. The regions of highest slip are very shallow to the north and south of the coseismic slip zone and just off the northeast shore, where significant slip reaches to a maximum of $\sim$60 km depth.

A comparison of horizontal displacements for the assumed viscoelastic structure (Fig. 9a) and inferred residual afterslip (Fig. 9b) is shown in Figs. 10a and 10b, respectively. Horizontal displacements associated with the combined viscoelastic relaxation and afterslip models are compared to the observed displacements in Fig. 10c, and the residual displacements (observed minus combined calculated displacements) are shown in Fig. 10d. The corresponding comparisons for vertical displacements are shown in Fig. 11. This combined model can explain all of the observed postseismic displacements, on-land and offshore, horizontal and vertical (Figs. 10d and 11d).

Postseismic relaxation and afterslip have been assumed to be independent. In fact, afterslip itself will change the stress field, potentially resulting in an additional viscoelastic response. We explored this possibility by solving for the component of viscoelastic relaxation due to afterslip. This was accomplished by applying the inferred afterslip from model 19 in addition to the coseismic slip, but applied in a time-dependent manner with rate changes consistent with a typical displacement time-series (e.g., Fig. 2). In the northern region where afterslip postseismic surface displacements are greatest, the on-land viscoelastic relaxation component increases by less than 5% for this test, while in the southern region where afterslip is strongest, the on-land viscoelastic relaxation component increases by a less than 1%. The northern afterslip leads to a larger viscoelastic response because it extends to just under the edge of the coast, while southern afterslip remains more offshore. In order to match the misfit of model 19, this would translate into a reduction in the deeper portion of the northern afterslip region by less than 3%.

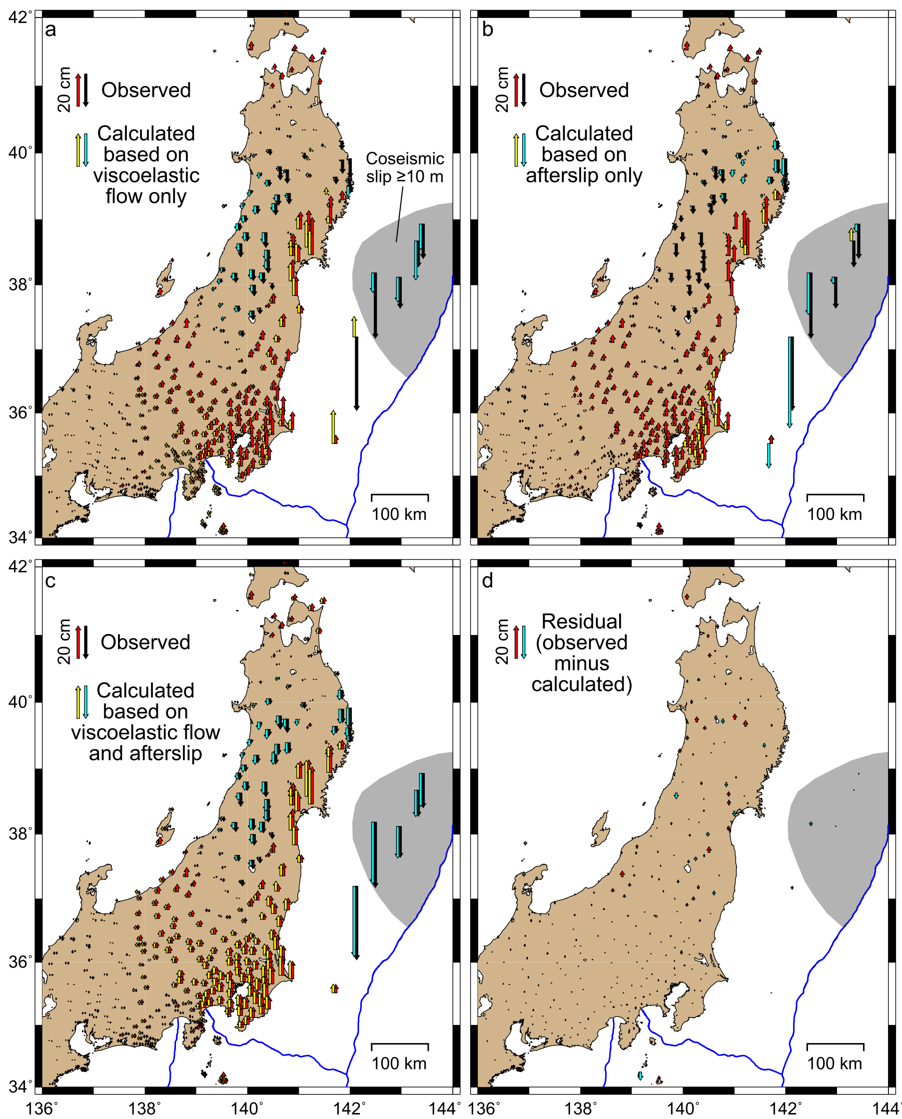

Fig. 11. Comparison of calculated and observed vertical displacements associated with (a) viscoelastic relaxation (viscosity structure shown in Fig. 9a) and (b) afterslip (afterslip distribution shown in Fig. 9b) associated with the best-fitting combined model (model 19 in Table 1). (c) Vertical displacements associated with the combined contributions viscoelastic relaxation and afterslip for the best-fitting model, and (d) the associated residual vertical displacements (observed minus combined calculated displacements).

We also explored the potential role of poroelastic rebound, the process by which pressure changes associated with coseismic slip drives fluids to migrate within the crust, causing postseismic displacements. Poroelastic flow can be modeled by taking the difference between two elastic coseismic solutions with varying Poisson's ratio's (e.g. Peltzer et al., 1996, 1998). Following the methodology of Hu et al. (2014), we modeled a 10 km thick poroelastic layer in the slab and a 6 km layer in the continental crust. We assumed Poisson's ratios of 0.31 and 0.25 for the drained and undrained conditions, respectively. Our results suggest that poroelastic rebound would influence on-land horizontal and vertical displacements near the coast by less than 1 cm (cf. Hu et al., 2014). Poroelastic rebound may have influenced the postseismic displacements in the area of the seafloor measurements by as much as 3 cm. While we cannot rule out a more significant influence of poroelastic rebound on seafloor displacements, such an effect would likely only modestly change the shallow portion of our inferred afterslip slip distribution, substantiating Sun et al.'s (2014) conclusion that poroelastic rebound cannot be the primary source of westward directed seafloor velocities.

5. Discussion

Our results suggest that postseismic surface displacements following the 2011 Tohoku-oki earthquake are due to about equal parts viscoelastic relaxation and afterslip, though the contributions from each vary spatially. In general, viscoelastic relaxation is more dominant on-land in the same latitude range as the coseismic slip, where afterslip is more dominant to the north and south of this region. This is also generally true off-shore. Our results suggest that both mechanisms are active immediately after a large megathrust earthquake.

Viscoelastic relaxation is dominated by a low viscosity, layered mantle wedge (Fig. 9a). This is in contrast to previous studies, which assumed a mantle wedge with a uniform viscosity (Diao et al., 2014; Hu et al., 2014, 2016; Shirzaei et al., 2014; Sun et al., 2014, 2015; Yamagiwa et al., 2015). Our inferred structure has the lowest viscosity between 150 and 300 km depth, which is consistent with a weak asthenospheric region due to the opposing influences of increasing temperatures and pressure with depth (e.g., Hirth and Kohlstedt, 2003). Similar to previous work, the mantle wedge atop the slab is found to be about an order of magnitude weaker than the oceanic mantle underneath the subducting plate to the east. This is consistent with the mantle wedge being wetter than regular mantle due to volatile release from the subducting slab (e.g., Hirth and Kohlstedt, 2003).

One of the more surprising results is that no lateral heterogeneities within the mantle wedge are required to explain the postseismic data despite the fact that temperatures within the wedge cool near the slab and there is a volcanic arc that runs down the western half of the island. One possibility is that closer to the slab, the influence of cooler temperatures on viscosity are offset by a higher water content. And perhaps the lowering of viscosity due to the presence of melt is offset by the removal of water from the surrounding source mantle. While it is doubtful that such offsets would be so well balanced, these tradeoffs may be sufficient with respect to the viscosity resolution of the present analysis. In particular, one need not appeal to a special case of a zone of weakness associated with the volcanic arc (Hu et al., 2014) to explain the postseismic subsidence that occurs in this region—it arises from the combination of a layered wedge rheology interacting with the geometry of the subducting slab.

Westward directed postseismic displacements on the seafloor are a result of viscoelastic relaxation directly below the coseismic slip region. However, our analysis is not sensitive enough to determine whether this weakness arises from a thin (order 10 km), weak sublithospheric layer, perhaps due to pooled melts (Sun et al., 2014), or within the lower half of the Pacific lithosphere due to high stresses associated with plate bending. The thin, sublithospheric layer scenario requires more than an order of magnitude lower viscosity (10^{17} Pa s) compared to the weak lower slab scenario because of the narrowness and depth of the layer. This means that the sublithospheric layer should fully relax coseismic stresses much faster—our model would estimate within 5 years following the earthquake. Thus, if the sublithospheric scenario is correct, then we should see the westward velocities vanish soon. At the writing of this manuscript, seafloor data is not available for this time frame, and thus a conclusion cannot be drawn.

Our inferred afterslip distribution generally occurs in the area surrounding the coseismic slip region, where coseismic stress increases would be greatest. Consistent with previous Tohoku-oki postseismic studies, there is some overlap of afterslip with the region of coseismic slip, which implies that within this area interface stresses were not totally relieved by coseismic slip (Diao et al., 2014; Perfettini and Avouac, 2014; Yamagiwa et al., 2015). To the north, this slip lies in a corridor that extends from the trench to ~60 km depth, flanked by the inferred source regions of historical tsunamis (Hashimoto et al., 2009). These source regions are areas of inferred uplift that reflect the extent of slip associated with these historic earthquakes. These could represent strong asperities on the plate interface that act as barriers to afterslip following the Tohoku-oki earthquake. To the south, these tsunami source regions appear to act as a barrier preventing afterslip from penetrating deeper along the interface compared to the northern region.

The two largest interplate aftershocks to follow the Tohoku-oki earthquake are located at the boundary of the inferred afterslip (denoted as green stars in Fig. 9b), suggesting that the aftershocks may have had a significant influence on postseismic deformation (or vice-versa). We calculated the expected postseismic displacements based on our best-fitting viscoelastic structure (Fig. 9a). The M7.3 northern aftershock was inferred to have occurred on the plate interface (30 km depth) with 1.7 m of slip on a 40 km × 35 km patch, while the southern M7.7 southern aftershock was inferred to occur on the plate interface (35 km deep) with 3.7 m of slip on a 61 km × 59 km patch (Nishimura et al., 2011). We found that both aftershocks would have had less than a 1% influence on observed postseismic displacements.

6. Conclusions

Our viscoelastic model of the M9 2011 Tohoku-oki, Japan earthquake provides a solution that explains all on-land and seafloor horizontal and vertical postseismic displacements. It does so in a manner that is consistent with a mantle rheology that is influenced by temperature, pressure, and water content, and an afterslip distribution that occurs primarily in the space between the Tohoku-oki slip region and the source regions of historic tsunamis. Westward seafloor postseismic displacements are either due to viscoelastic relaxation in the lower half of the Pacific lithosphere being weakened by plate bending, or within a thin, weak sublithospheric layer. Our results suggest that the subduction of the Philippine Sea Plate extends to only ~100 km depth in the study region. We find that Tohoku-oki postseismic displacements are about equal parts due to viscoelastic relaxation and afterslip, but spatially distinct. This goes against the paradigm by which afterslip is thought of as the most influential postseismic mechanism immediately following earthquakes, with viscoelastic relaxation to follow only in later years.

Acknowledgements

We thank two anonymous reviewers for thoughtful comments that improved the manuscript. Support in the USA was provided by the National Science Foundation through grants EAR-1215358 (AMF) and EAR-1215757 (TWB, DAO). Support within Japan was provided by the Special Project for Reducing Vulnerability for Urban Mega Earthquake Disasters, the Integrated Research Project on Seismic and Tsunami Hazards Around the Sea of Japan, and the Earthquake and Volcano Hazards Observation and Research Program from the Ministry of Education, Culture, Sports, Science, and Technology of Japan (AH and HS). Additional support in Japan was provided by the Japan Ministry of Land, Infrastructure and Transport (YH). Most figures were generated using GMT (Wessel and Smith, 1998).

References

Apel, E., Bürgmann, R., Steblov, G., Vasilenko, N., King, R., Prytkov, A., 2006. Active tectonics of northeast Asia: using GPS velocities and block modeling to test independent Okhotsk plate motion. Geophys. Res. Lett. 33. http://dx.doi.org/10.1029/2006GL026077.

Baba, T., Tanioka, Y., Cummins, P.R., Uhira, K., 2002. The slip distribution of the 1946 Nankai earthquake estimated from tsunami inversion using a new plate model. Phys. Earth Planet. Inter. 132, 59–73.

Buffett, B.A., Becker, T.W., 2012. Bending stress and dissipation in subducted lithosphere. J. Geophys. Res. 117, B05413. http://dx.doi.org/10.1029/2012JB009205.

Bürgmann, R., Dresen, G., 2008. Rheology of the lower crust and upper mantle: evidence from rock mechanics, geodesy, and field observations. Annu. Rev. Earth Planet. Sci. 36, 531–567.

Diao, F., Xiong, X., Wang, R., Zheng, Y., Walter, T.R., Weng, H., Li, J., 2014. Overlapping post-seismic deformation processes: afterslip and viscoelastic relaxation following the 2011 Mw 9.0 Tohoku (Japan) earthquake. Geophys. J. Int. 196, 218–229. http://dx.doi.org/10.1093/gji/ggt376.

Freed, A.M., Bürgmann, R., 2004. Evidence of power-law flow in the Mojave Desert mantle. Nature 430, 548–551.

Freed, A.M., Bürgmann, R., Calais, E., Freymueller, J., Hreinsdóttir, S., 2006. Implications of deformation following the 2002 Denali, Alaska, earthquake for postseismic relaxation processes and lithospheric rheology. J. Geophys. Res. 111, B01401. http://dx.doi.org/10.1029/2005JB003894.

Freed, A.M., Bürgmann, R., Herring, T., 2007. Far-reaching transient motions after Mojave earthquakes require broad mantle flow beneath a strong crust. Geophys. Res. Lett. 34. http://dx.doi.org/10.1029/2007GL030959.

Freed, A.M., Hirth, G., Behn, M.D., 2011. Using short-term postseismic displacements to infer the ambient deformation conditions of the upper mantle. J. Geophys. Res. 117 (B1). http://dx.doi.org/10.1029/2011JB008562.

Hashimoto, C., Noda, A., Sagiya, T., Matsu'ura, M., 2009. Interplate seismogenic zones along the Kuril–Japan trench inferred from GPS data inversion. Nat. Geosci. 2, 141–144.

Hayes, G.P., Wald, D.J., Johnson, R.L., 2012. Slab1.0: a three-dimensional model of global subduction zone geometries. J. Geophys. Res. 117, B01302. http://dx.doi.org/10.1029/2011JB008524.

Hearn, E.H., Bürgmann, Roland, 2005. The effect of elastic layering on inversions of GPS data for coseismic slip and resulting stress changes: strike-slip earthquakes. Bull. Seismol. Soc. Am. 95, 1637–1653. http://dx.doi.org/10.1785/0120040158.

Hirose, F., Nakajima, J., Hasegawa, A., 2008a. Three-dimensional seismic velocity structure and configuration of the Philippine Sea slab in southwestern Japan estimated by double-difference tomography. J. Geophys. Res. 113, B09315. http://dx.doi.org/10.1029/2007JB005274.

Hirose, F., Nakajima, J., Hasegawa, A., 2008b. Three-dimensional velocity structure and configuration of the Philippine Sea slab beneath Kanto district, central Japan, estimated by double-difference tomography. J. Seismol. Soc. Jpn. 60, 123–138 (in Japanese with English abstract).

Hirth, G., Kohlstedt, D.L., 2003. Rheology of the upper mantle and the mantle wedge: a view from the experimentalists. In: Eiler, J. (Ed.), The Subduction Factory. In: Geophys. Monogr. Ser., vol. 138, pp. 83–102.

Hu, Y., Bürgmann, R., Freymueller, J.T., Banerjee, P., Wang, K., 2014. Contributions of poroelastic rebound and a weak volcanic arc to the postseismic deformation of the 2011 Tohoku earthquake. Earth Planets Space 66, 106. http://dx.doi.org/10.1186/1880-5981-66-106.

Hu, Y., Bürgmann, R., Uchida, N., Banerjee, P., Freymueller, J.T., 2016. Stress-driven relaxation of heterogeneous upper mantle and time-dependent afterslip following the 2011 Tohoku earthquake. J. Geophys. Res., Solid Earth 120. http://dx.doi.org/10.1002/2015JB012508.

Iinuma, T., Hino, R., Kido, M., Inazu, D., Osada, Y., Ito, Y., Ohzono, M., Tsushima, H., Suzuki, S., Fujimoto, H., Miura, S., 2012. Coseismic slip distribution of the 2011 off the Pacific Coast of Tohoku Earthquake (M9.0) refined by means of seafloor geodetic data. J. Geophys. Res. 117, 976 B07409. http://dx.doi.org/10.1029/2012JB009186.

Kita, S., Okada, T., Hasegawa, A., Nakajima, J., Matsuzawa, T., 2010. Anomalous deepening of a seismic belt in the upper-plane of the double seismic zone in the Pacific slab beneath the Hokkaido corner: possible evidence for thermal shielding caused by subducted forearc crust materials. Earth Planet. Sci. Lett. 290, 415–426.

Kyriakopoulos, C., Masterlark, T., Stramondo, S., Chini, M., Bignami, C., 2013. Coseismic slip distribution for the Mw 9 2011 Tohoku-Oki earthquake derived from 3-D FE modeling. J. Geophys. Res., Solid Earth 118, 3837–3847. http://dx.doi.org/10.1002/jgrb.50265.

Lin, Y.-n.N., et al., 2013. Coseismic and postseismic slip associated with the 2010 Maule Earthquake, Chile: characterizing the Arauco Peninsula barrier effect. J. Geophys. Res., Solid Earth 118, 3142–3159. http://dx.doi.org/10.1002/jgrb.50207.

Matsubara, M., Obara, K., Kasahara, K., 2008. Three-dimensional P- and S-wave velocity structures beneath the Japan Islands obtained by high-density seismic stations by seismic tomography. Tectonophysics 454, 86–103.

Nakajima, J., Hasegawa, A., 2006. Anomalous low-velocity zone and linear alignment of seismicity along it in the subducted Pacific slab beneath Kanto, Japan: reactivation of subducted fracture zone? Geophys. Res. Lett. 33, L16309. http://dx.doi.org/10.1029/2006GL026773.

Nakajima, J., Hasegawa, A., 2007. Subduction of the Philippine Sea plate beneath southwestern Japan: slab geometry and its relationship to arc magmatism. J. Geophys. Res. 112, B08306. http://dx.doi.org/10.1029/2006JB004770.

Nakajima, J., Hirose, F., Hasegawa, A., 2009. Seismotectonics beneath the Tokyo metropolitan area, Japan: effect of slab-slab contact and overlap on seismicity. J. Geophys. Res. 114, B08309. http://dx.doi.org/10.1029/2008JB006101.

Nishimura, T., Munekane, H., Yarai, H., 2011. The 2011 off the Pacific coast of Tohoku Earthquake and its aftershocks observed by GEONET. Earth Planets Space 63, 631–636.

Ozawa, S., et al., 2012. Preceding, coseismic, and postseismic slips of the 2011 Tohoku earthquake, Japan. J. Geophys. Res. 117, B07404.

Peacock, S.M., Wang, K., 1999. Seismic consequences of warm versus cool subduction metamorphism: examples from southwest and northeast Japan. Science 286, 937–939.

Peltzer, G., Rosen, P., Rogez, F., Hudnut, K., 1996. Postseismic rebound in fault stepovers caused by pore fluid flow. Science 273, 1202–1204.

Peltzer, G., Rosen, P., Rogez, F., Hudnut, K., 1998. Poroelastic rebound along the Landers 1992 earthquake surface rupture. J. Geophys. Res. 103, 30131–30145. http://dx.doi.org/10.1029/98JB02302.

Perfettini, H., Avouac, J.P., 2014. The seismic cycle in the area of the 2011 Mw9.0 Tohoku-Oki earthquake. J. Geophys. Res., Solid Earth 119, 4469–4515. http://dx.doi.org/10.1002/2013JB010697.

Pollitz, F.F., 2003. Transient rheology of the uppermost mantle beneath the Mojave Desert, California. Earth Planet. Sci. Lett. 215, 89–104.

Pulvirenti, F., Shuanggen, J., Aloisi, M., 2014. An adjoint-based FEM optimization of coseismic displacements following the 2011 Tohoku earthquake: new insights for the limits of the upper plate rebound. Earth Planet. Sci. Lett. 237, 25–39.

Sella, G.F., Dixon, T.H., Mao, A., 2002. REVEL: a model for recent plate velocities from space geodesy. J. Geophys. Res. 107, 2081. http://dx.doi.org/10.1029/2000JB000033.

Shirzaei, M., Bürgmann, R., Uchida, N., Hu, Y., Pollitz, F., Matsuzawa, T., 2014. Seismic versus aseismic slip: probing mechanical properties of the northeast Japan subduction zone. Earth Planet. Sci. Lett. 406, 7–13.

Sun, T., et al., 2014. Prevalence of viscoelastic relaxation after the 2011 Tohoku-oki earthquake. Nature 514, 84–87.

Sun, T., Wang, K., 2015. Viscoelastic relaxation following subduction earthquakes and its effects on afterslip determination. J. Geophys. Res., Solid Earth 120, 1329–1344. http://dx.doi.org/10.1002/2014JB011707.

Syracuse, E.M., van Keken, P.E., Abers, G.A., 2010. The global range of subduction zone thermal models. Phys. Earth Planet. Inter. 183, 73–90.

Tajima, F., Mori, J., Kennett, B.L., 2013. A review of the 2011 Tohoku-Oki earthquake (Mw 9.0): large-scale rupture across heterogeneous plate coupling. Tectonophysics 586, 15–34.

Wang, K., Hu, Y., He, J., 2012. Deformation cycles of subduction earthquakes in a viscoelastic Earth. Nature 484, 327–332.

Watanabe, S., Sato, M., Fujita, M., Ishikawa, T., Yokota, Y., Ujihara, N., Asada, A., 2014. Evidence of viscoelastic deformation following the 2011 Tohoku-Oki earthquake revealed from seafloor geodetic observation. Geophys. Res. Lett. 41, 5789–5796. http://dx.doi.org/10.1002/2014GL061134.

Wessel, P., Smith, W.H.F., 1998. New improved version of the Generic Mapping Tools released. Eos Trans. AGU 79, 579.

Wiseman, K., Bürgmann, R., Freed, A.M., 2015. Viscoelastic relaxation in a heterogeneous Earth following the 2004 Sumatra–Andaman earthquake. Earth Planet. Sci. Lett. 431, 308–317.

Yamagiwa, S., Miyazaki, S., Hirahara, K., Fukahata, Y., 2015. Afterslip and viscoelastic relaxation following the 2011 Tohoku-oki earthquake (Mw9.0) inferred from inland GPS and seafloor GPS/Acoustic data. Geophys. Res. Lett. 42, 66–73. http://dx.doi.org/10.1002/2014GL061735.

Yamazaki, Y., Lay, T., Cheung, K.F., Yue, H., Kanamori, H., 2011. Modeling near-field tsunami observations to improve finite-fault slip models for the 11 March 2011 Tohoku earthquake. Geophys. Res. Lett. 38, L00G15. http://dx.doi.org/10.1029/2011GL049130.